Ranges of $^{15}N^+$ ions in ten metals measured by $(p, \alpha\gamma)$ resonance broadening

M. Luomajärvi, J. Keinonen, M. Bister, and A. Anttila
Department of Physics, University of Helsinki, Helsinki, Finland
(Received 1 February 1978)

Concentration distributions of $^{15}N^+$ ions implanted in Al, Ti, Ni, Cu, Zn, Mo, Ag, Ta, W, and Au substrates have been measured in the energy range of 20–100 keV by means of the broadening of the $E_p = 429$ keV resonance yield curve from the $^{15}N(p, \alpha\gamma)^{12}C$ reaction. The implanted-atom concentration was always less than 0.1%. The proton stopping powers needed in the derivation of the ranges were determined experimentally. Proton energy straggling was included in the ^{15}N range analysis. In comparing the distribution predictions of the Lindhard-Scharff-Schiøtt (LSS) theory with the experimental results the fraction of ^{15}N reflections was taken into account with the Monte Carlo calculations. The consistency between theoretical and experimental range values is within 20% limits. Except for the Al and Ti cases, the mean ranges in these polycrystalline targets were found to be larger than those predicted by the LSS theory as being valid for amorphous targets. The merits of the method used, the effects of possible diffusion, and relevance of the range values to Doppler-shift attenuation measurements are discussed.

I. INTRODUCTION

The large fluctuations of nuclear lifetimes obtained in Doppler-shift attenuation (DSA) measurements[1-3] demonstrate unpredicted fluctuations in the stopping-power values of different slowing-down materials. The scarcity of applicable experimental data on stopping powers or ranges in the literature reflects the variety of parameters needed to describe each application. Even the three main variables, the incoming ion, its energy, and the backing material, present a wide spectrum of possibilities. Furthermore, in many practical applications, high-purity polycrystalline metals are more suited, even though the theoretical values are derived only for amorphous materials. Consequently, one is forced to use the amorphous-backing theory as a conceptual framework within which to obtain stopping powers from range measurements, and then to see if these effective quantities are also appropriate for application, e.g., in DSA analysis.

In the present work, an earlier study of the ranges of $^{15}N^+$ ions in tantalum, needed for DSA measurements[4,5] is extended to a study of the range distributions of 20–100 keV $^{15}N^+$ ions in ten metals, some of which are possible candidates for DSA measurements. The aim was a systematic investigation of the dependence of the range values on the Z_2 value, varying from 13 to 79, and also to see the development of the fraction of reflection which distorts the infinite-target profile.

The use of the $E_p = 429$ keV $^{15}N(p, \alpha\gamma)^{12}C$ resonance broadening as a probing method requires the proton stopping power of each backing material to be known. Likewise, some estimation of possible ^{15}N diffusion should be made to reach reliable range values. For each measurement of ^{15}N range, proton stopping, and diffusion, a very-well-polished and contamination-free surface of the backing substrate is needed. The proton-stopping-power and diffusion measurements were performed in the laboratory at the same time as the range measurements, so that the preparation of backings could be coordinated and the results of the former measurements used to support the range values could be obtained.

The experimental procedure and measurements are described in Sec. II; Sec. III presents the results. The method used, the effects of possible radiation-enhanced diffusion, and the relevance of the range values to DSA measurements are discussed in Sec. IV.

II. EXPERIMENTAL PROCEDURE AND MEASUREMENTS

The broadening of the $E_p = 429$ keV $^{15}N(p, \alpha\gamma)^{12}C$ resonance yield curve was used to determine the range profiles of 20–100 keV $^{15}N^+$ ions. This method offers the possibility to measure the ranges easily, with sufficient accuracy, and, most important, without destroying the target.

The proton beam of about 2 μA was produced by the 2.5-MV Van de Graaff accelerator at the University of Helsinki. The energy resolution of the accelerator beam (about 350 eV) was determined from the thick target yield of the $E_p = 992$ keV $^{27}Al(p,\gamma)^{28}Si$ resonance, the natural width of this resonance being 100 eV.[6] The experimental energy resolution, calculated from the energy resolution of the accelerator and from the natural width, 0.9 keV,[7] of the $E_p = 429$ keV $^{15}N(p, \alpha\gamma)^{12}C$ resonance varied during the measurements from about 1.0 to

1.2 keV. The corresponding depth resolution depends on the proton stopping power involved and was typically about 7 nm. An energy window was used to count the 4.43-MeV γ rays from the E_p = 429 keV $^{15}N(p,\alpha\gamma)^{12}C$ reaction detected with a 12.7×10.2 cm^2 NaI(Tl) crystal.

The implanted ^{15}N targets were prepared from enriched nitrogen gas [$(97.7\pm0.1)\%$ ^{15}N according to the manufacturer's statement] using the electromagnetic isotope separator at the University of Helsinki. The backings were commercially available rolled-metal plates, with thicknesses about 0.3 mm (Mo, Ta, W, Au) or about 1 mm (Al, Ti, Ni, Cu, Zn, Ag), and purities (according to the statements of the manufacturer's) better than 99.9% in all cases. The Al, Ti, Ni, Cu, Zn, and Ag plates were first polished mechanically, after which all plates were electropolished[8] and thoroughly cleaned. The concentrations of the implanted atoms were kept as low as possible to avoid distortion of the range distributions due to the stopping power of the earlier implanted ions which is a cumulative effect.[9] Due to the large cross section of the E_p = 429 keV $^{15}N(p,\alpha\gamma)^{12}C$ reaction,[7] the ^{15}N concentration below 0.1% was in all cases enough to yield sufficient statistical accuracy for the γ-ray counts describing the range distribution. To avoid any effect of implantation energy errors, two sets of targets were prepared, each set containing implantations at the energies 20, 40, 60, 80, and 100 keV. The $^{15}N^+$ ions were implanted at normal incidence. To eliminate the errors in the range values arising from the target texture, a further two sets of targets were prepared where the targets were tilted 6° relative to the normal of incidence. All implantations were performed at the room temperature.

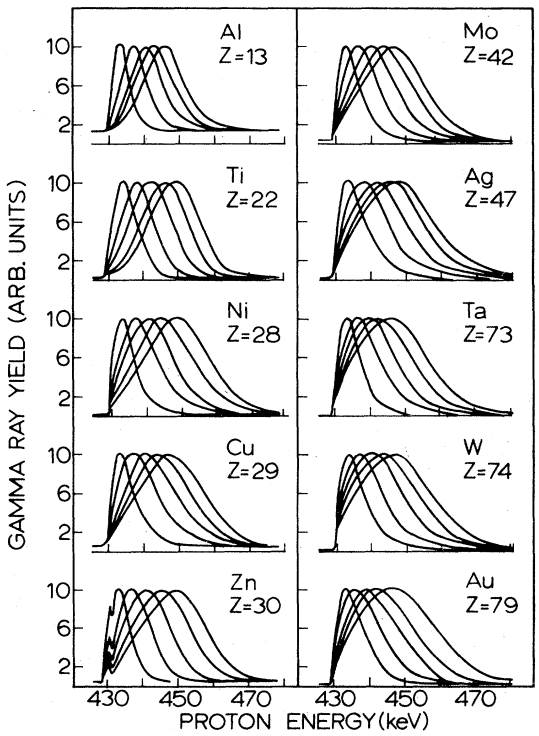

FIG. 1. γ-ray yield curve from the $^{15}N^+$ implantations into ten different metals. The peak heights are normalized to the same value. The peak height value at the maximum varied between 3000 and 10 000 counts for the proton charge of 15–60 μC taken at every point.

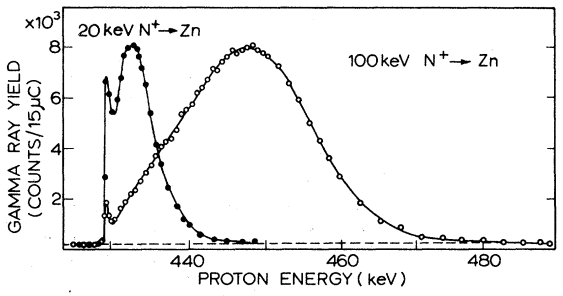

FIG. 2. Same γ-ray yield curves for the 20 and 100 keV $^{15}N^+$ → Zn cases as in Fig. 1, but with enlarged scale to illustrate the surface peaks.

During the $^{15}N(p,\alpha\gamma)^{12}C$ yield measurements the angle of proton incidence was the same as for $^{15}N^+$ ions during the implantations. No texture effects between the two series of targets were seen. As a rule, the yield measurements were performed twice with every target. The reducibility of the yield measurements and thus the range profiles were within statistical errors. In the vacuum of about 50 μPa, there was no carbon-contamination distortion on the relatively short-yield measurements.

The γ-ray yield curves as obtained in the measurements are shown in Fig. 1. The concentration peaks seen in the front edges of the implantation profiles for Zn are illustrated in more detail in Fig. 2. Excluding the small effects noticeable for Ni and Cu, the other ^{15}N distribution profiles were free from this kind of peak. The proton bombardment neither produced nor destroyed these peaks; the effects of this radiation enhanced diffusion on the range values will be discussed in Sec. IV. Nor did the proton bombardment induce any change in the range profiles.

III. RESULTS

The broadening of the E_p = 429 keV $^{15}N(p,\alpha\gamma)^{12}C$ resonance yield curves, as illustrated in Fig. 1, give directly fairly good representations of the concentration distributions of the implanted $^{15}N^+$ ions. In a more accurate range determination,

TABLE I. Ranges of $^{15}N^+$ ions in $_{13}$Al, $_{22}$Ti, $_{28}$Ni, $_{29}$Cu, $_{30}$Zn, $_{42}$Mo, $_{47}$Ag, $_{73}$Ta, $_{74}$W, and $_{79}$Au compared with calculated values.

Backing	Energy (keV)	$\bar{R}_{obs}$ (μg/cm^2)	$\bar{R}_{obs}/\bar{R}_{MC}$ [a]	Backing	Energy (keV)	$\bar{R}_{obs}$ (μg/cm^2)	$\bar{R}_{obs}/\bar{R}_{MC}$
Al	20	14.5 ± 1.5	1.13 ± 0.12	Mo	20	34 ± 2	1.33 ± 0.08
	40	28 ± 2	1.07 ± 0.08		40	53 ± 3	1.14 ± 0.06
	60	40 ± 2	1.01 ± 0.05		60	74 ± 3	1.08 ± 0.04
	80	53 ± 3	1.01 ± 0.06		80	94 ± 3	1.05 ± 0.03
	100	63 ± 3	0.96 ± 0.05		100	115 ± 4	1.03 ± 0.04
Ti	20	17.7 ± 1.5	1.05 ± 0.09	Ag	20	39 ± 2	1.42 ± 0.07
	40	33 ± 2	0.91 ± 0.06		40	63 ± 3	1.25 ± 0.06
	60	47 ± 2	0.92 ± 0.04		60	84 ± 3	1.15 ± 0.04
	80	62 ± 3	0.91 ± 0.04		80	105 ± 4	1.10 ± 0.04
	100	75 ± 3	0.88 ± 0.04		100	123 ± 5	1.04 ± 0.04
Ni	20	25 ± 2	1.38 ± 0.11	Ta	20	48 ± 2	1.17 ± 0.05
	40	45 ± 2	1.22 ± 0.05		40	80 ± 3	1.13 ± 0.04
	60	61 ± 3	1.11 ± 0.05		60	112 ± 4	1.12 ± 0.04
	80	82 ± 3	1.12 ± 0.04		80	139 ± 5	1.09 ± 0.04
	100	98 ± 3	1.07 ± 0.03		100	166 ± 5	1.07 ± 0.03
Cu	20	29.0 ± 1.5	1.49 ± 0.08	W	20	56 ± 2	1.34 ± 0.05
	40	51 ± 3	1.33 ± 0.08		40	91 ± 3	1.29 ± 0.04
	60	71 ± 3	1.26 ± 0.05		60	128 ± 4	1.26 ± 0.04
	80	88 ± 3	1.17 ± 0.04		80	155 ± 6	1.19 ± 0.05
	100	104 ± 4	1.11 ± 0.04		100	181 ± 6	1.17 ± 0.04
Zn	20	23.0 ± 1.5	1.18 ± 0.08	Au	20	59 ± 3	1.35 ± 0.07
	40	46 ± 2	1.20 ± 0.05		40	96 ± 4	1.36 ± 0.06
	60	67 ± 3	1.20 ± 0.05		60	130 ± 5	1.25 ± 0.05
	80	89 ± 3	1.19 ± 0.04		80	167 ± 6	1.24 ± 0.04
	100	110 ± 4	1.18 ± 0.04		100	203 ± 8	1.28 ± 0.05

[a] Error limits are calculated from the errors limits of $\bar{R}_{obs}$.

however, the energy distribution of the proton beam, its energy straggling within the target, and the natural width of the resonance should be taken into account. The determination of an experimental mean range from a measured concentration distribution is described analytically in an earlier paper.[10] The centroid positions of the concentration distributions obtained directly from the yield curves showed the dependence between the $^{15}N^+$ ion ranges and the proton stopping powers at E_p = 429 keV. There appears to be no systematic dependence on the Z_2 values, but rather the values coincide within ±10% of the average value at each energy. Using the stopping powers 262 ± 9, 221 ± 8, 191 ± 7, 171 ± 4, 167 ± 6, 152 ± 5, 142 ± 4, 96 ± 3, 95 ± 3, and 91 ± 3 keV/mg of Al, Ti, Ni, Cu, Zn, Mo, Ag, Ta, W, and Au, respectively, for 429 keV protons,[11] the mean ranges given in the third column of Table I were obtained. The indicated error limits include the error limits of the centroid positions of the concentration distributions evaluated from the scatter of the results obtained at different times and with different targets, and the error limits of the proton stopping power values. In Fig. 3 the results of Table I are presented graphically, where it can be seen that the ranges in this energy region depend almost linearly on the implantation energy.

In comparing the measured range distributions with theory, it is necessary to take into account the reflection of $^{15}N^+$ ions from the target during the implantation, especially for low-energy ions implanted into heavy materials (Fig. 1). To take the surface of the backing material into account in a realistic way, we have calculated the range profiles by a Monte Carlo program[12] for semi-infinite targets, and to assess the importance of the inclusion of the target surface, the range profiles have been calculated for some cases in infinite targets (Fig. 4). In the calculations, the LSS scattering cross sections[13] were used. The shaded areas in Fig. 4 represent the reflected ions and it is seen that the distortion of the infinite target profile by the surface is fundamental in heavier materials, even at high implantation energies. The comparison of the experimental results given in the third column of Table I with the values obtained from LSS theory,[13] $\bar{R}_{MC}$, with the inclusion of the sur-

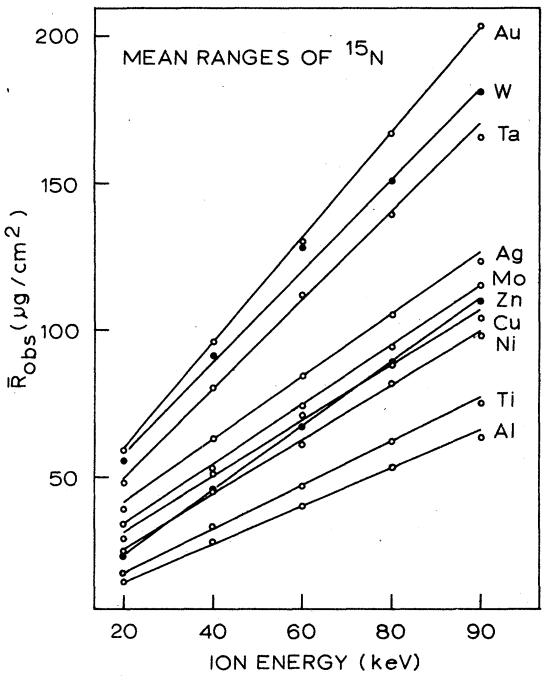

FIG. 3. Observed mean ranges in units of $\mu g/cm^2$. (The lines are drawn to guide the eye.)

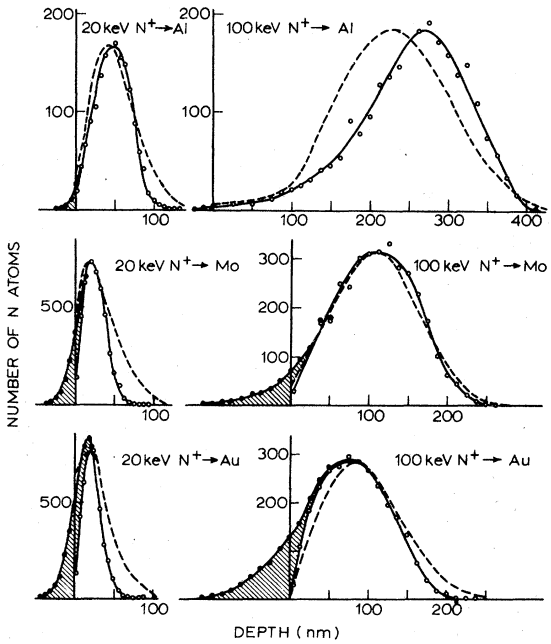

FIG. 4. Range distributions calculated for 20 and 100 keV $^{15}N^+$ ions in Al, Mo, and Au by using LSS scattering cross sections in Monte Carlo calculations. The solid line with open circles gives the result corresponding to the experimental one (the dashed line). The filled dots correspond to the case calculated for the infinite medium. The shaded area gives the fraction of reflected particles.

face, are given in the fourth column of Table I. It can be seen that in almost all cases, except Al and Ti, the experimental ranges in the polycrystalline targets are somewhat greater than the theoretical ones calculated using amorphous material assumptions. However, this effect is not so high that the $\bar{R}_{obs}/\bar{R}_{MC}$ ratios could be grouped according to the lattice type: the fcc metals Al, Ni, Cu, Ag, Au, bcc metals Mo, Ta, W, and hcp metals Ti, Zn show no systematic dependence of the ratios on lattice type. The oscillations of the $\bar{R}_{obs}/\bar{R}_{MC}$ ratios as the function of Z_2 are briefly discussed in Sec. IV.

IV. DISCUSSION

The large cross section of the $E_p = 429$ keV ^{15}N $(p, \alpha\gamma)^{12}C$ resonance[7] makes the method used very suitable for the determination of range distributions; the proton beam intensity and energy resolution, and the γ-ray detection efficiency present only minor experimental difficulties. The more common chemical peeling method, where radioactive ions are used, and the use of a secondary-ion mass spectrometry would lead to better results especially in an accurate determination of the tail of the distribution. However, the nuclear reaction method is the only nondestructive way to generate data on concentration distributions. Hence, the measurements can be repeated several times in the same spot of the substrate in order to verify the reproducibility, which indisputably confirms the reliability. Rutherford back scattering, which is often used to measure range distributions, can only be applied easily to cases where the backing element is lighter than the impurity element.

During the ^{15}N implantation into the Zn, Cu, and Ni backings the radiation enhanced diffusion gives rise to surface peaks. In the analysis, an attempt was made to eliminate the effects of these peaks by extrapolating the concentration distribution to the surface in such a way as to leave out the peaked distribution near the surface. This is perhaps an uncertain approximation but it is the only way to eliminate the peak from the analysis. As was seen in Fig. 2, the radiation-enhanced diffusion can be crucial for low-energy ranges but not for high-energy ones. Being connected to the radiation-damage spikes, the radiation-enhanced diffusion cannot be avoided during the implantations. Experimentally, one would minimize the diffusion by cooling the target during the implantation. However, when cooling the polycrystalline material, for example to the liquid-nitrogen temperature, one should consider the effects of the reduced atomic vibrations on the channeling probabilities.[14] Consequently, our needs are to find and use reliable backing materials for DSA measurements to

be performed at the room temperature.

The study of the diffusion of nitrogen in the metals used in the present work is still in progress in our laboratory,[15] and although the complete picture is not yet available, a few points are worth noting at this stage. In the case of Zn, as can be expected,[16] a high diffusion factor has been obtained.[17] Thus, the ranges obtained should be considered to be influenced by this "systematic error" unobservable in the error limits given. The anomalies of the $^{15}N^+$→Zn cases, especially in the low-energy ranges, relative to the systematics illustrated in Fig. 3, are very probably due to the diffusion. However, it should be pointed out that usually the discrepancies between the theoretical and experimental range distributions, such as the 20-keV $^{15}N^+$→Mo case, cannot be explained by a diffusion process. The nitrogen diffusion in molybdenum is measured to be out-diffusion,[18] and thus such diffusion, which was not observed in the range measurements, would "correct" the experimental profile to give better agreement with theory. Referring to the systematics of the values of Table I and to the Fig. 3, one can conclude that any possible diffusion which would have had a high effect on low-energy range values is very improbable in most cases studied in the present work.

The lifetimes of many nuclear states, being in the femtosecond region, can be measured only with the DSA technique, and the stopping power of the slowing-down material is needed in the analysis of the experimental results. The fit of the theoretical range, derived from the LSS theory[13] can be improved if the usual correction factors f_n and f_e, yielding the corrected stopping power $(d\epsilon/d\rho)_{corr} = f_n(d\epsilon/d\rho)_n^{LSS} + f_e(d\epsilon/d\rho)_e^{LSS}$, are adjusted according to the method presented in Ref. 19, where in addition to the range measurements DSA measurements should be done. In practice, however, one is forced to use polycrystalline targets which can withstand the fluxes required in DSA measurements. Thus, the problem appears that many of the ions moving under near-channeling conditions with reduced stopping and scattering for some portions of their paths can yield a broader distribution with a longer tail than predicted by the theory developed for amorphous material. Hence, a few details remain, which are not, however, importtant, since in the DSA analysis it is the mean value for the stopping which is important. The reliability of effective stopping powers as well as the absence of serious sources of error are confirmed by our previous work,[2] where lifetime values obtained using the measured range values are in good agreement with those obtained from resonance fluorescence and high-recoil measurements.

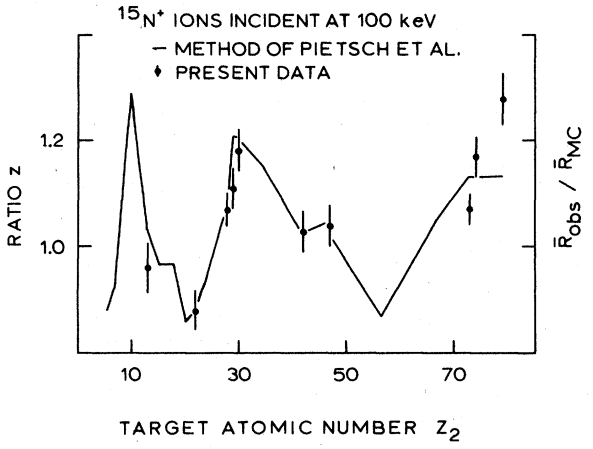

FIG. 5. Comparison of the fluctuations of the electronic stopping power produced with the modified Lindhard-Scharff method with the $\bar{R}_{obs}/\bar{R}_{MC}$ ratios for 100-keV $^{15}N^+$ ions from the fourth column of Table I.

In the first stage of the range analysis the centroid positions of the concentration distributions are obtained in kilo-electron-volts units of proton energy. These values happen to be consistent within 10% limits. This fact indicates the stopping dependence of the $E_p = 429$ keV protons and 20–100 keV $^{15}N^+$ ions, although in the former case the electronic stopping dominates and in the latter the nuclear stopping. This completely artificial comparison of nuclear and electronic stopping in the case of $^{15}N^+$ ions can be taken one step further. In the case of 800-keV $^{14}N^+$ ions, Land *et al.*[20] have modified the Lindhard and Scharff[21] model for electronic stopping power with the inclusion of atomic structure as proposed by Pietsch *et al.*[22] As in Ref. 20, we have fitted the Hartree-Fock-Slater screening factor to the Thomas-Fermi screening factor and have calculated the ratio $z = (Z_1^{2/3} + Z_2^{2/3})^{3/2}/(\alpha_1^2 Z_1^{2/3} + \alpha_2^2 Z_2^{2/3})^{3/2}$ as a function of Z_2. The ratios of experimental ranges $\bar{R}_{obs}$ to the calculated ones $\bar{R}_{MC}$ as given in the fourth column of Table I for 100-keV $^{15}N^+$ ions are compared in Fig. 5 with the calculated ratios z. The correction factor α_1 is normalized to yield $z = 1.03$ at $Z_2 = 42$. The oscillations of the $\bar{R}_{obs}/\bar{R}_{MC}$ ratios are similar also for lower implantation energies as can be seen in Table I. The fluctuations of the electronic stopping dependent on the atomic structure, and the fluctuations of the nuclear stopping obtained in LSS units from experimental data show unexpected good agreement. This is understandable partly because the nuclear stopping is also effected by the screening.

[1]C. Broude, P. Engelstein, M. Popp, and P. N. Tandon, Phys. Lett. B 39, 184 (1972).
[2]A. Anttila, M. Bister, and J. Keinonen, Z. Phys. A 274, 227 (1975).
[3]M. Toulemonde and F. Haas, Phys. Rev. C 15, 49 (1977).
[4]M. Bister, A. Anttila, and J. Keinonen, Phys. Rev. C 16, 1303 (1977).
[5]J. Keinonen, M. Bister, and A. Anttila, Nucl. Phys. A 286, 505 (1977).
[6]P. M. Endt and C. van der Leun, Nucl. Phys. A 214, 1 (1973).
[7]F. Ajzenberg-Selove, Nucl. Phys. A 268, 1 (1976).
[8]W. J. McG. Tegart, *The Electrolytic and Chemical Polishing of Metals in Research and Industry* (Pergamon, Belfast, 1959).
[9]M. Bister, A. Anttila, A. Fontell, and E. Leminen, Z. Phys. 250, 82 (1972).
[10]A. Anttila, M. Bister, A. Fontell, and K. B. Winterbon, Radiat. Eff. 33, 13 (1977).
[11]M. Luomajärvi (unpublished).
[12]M. Bister (unpublished).
[13]J. Lindhard, M. Scharff, and H. E. Schiøtt, K. Dan. Vidensk. Selsk. Mat. Fys. Medd. 33, 14 (1963).
[14]J. L. Whitton, in *Channeling, Theory, Observation and Applications*, edited by D. V. Morgan (Wiley, London, 1973), p. 225.
[15]J. Hirvonen and A. Anttila, Scr. Metall. (to be published).
[16]Metals Reference Book, edited by C. I. Smithells (Butterworths, London, 1976), p. 880.
[17]J. Hirvonen (unpublished).
[18]A. Anttila and J. Hirvonen (unpublished).
[19]M. Bister, A. Anttila, and J. Keinonen, Phys. Lett. 53 A, 471 (1975).
[20]D. J. Land, J. G. Brennan, D. J. Simmons, and M. D. Brown, Phys. Rev. A 16, 492 (1977).
[21]J. Lindhard and M. Scharff, Phys. Rev. 124, 128 (1961).
[22]W. Pietsch, U. Hauser, and W. Neuwirth, Nucl. Instrum. Methods 132, 79 (1976).